Understanding the high voltage behavior of LiNiO2 through the electrochemical properties of the surface layer

Edgar Bautista Quisbert, François Fauth, Artem M Abakumov, Maxime Blangero, Marie Guignard, Claude Delmas

NANO · MICRO small
www.small-journal.com

Understanding the High Voltage Behavior of $LiNiO_2$ Through the Electrochemical Properties of the Surface Layer

Edgar Bautista Quisbert, François Fauth,* Artem M. Abakumov,* Maxime Blangero,* Marie Guignard,* and Claude Delmas**

Nickel-rich layered oxides are adopted as electrode materials for EV's. They suffer from a capacity loss when the cells are charged above 4.15 V versus Li/Li^+. Doping and coating can lead to significant improvement in cycling. However, the mechanisms involved at high voltage are not clear. This work is focused on $LiNiO_2$ to overcome the effect of M cations. Galvanostatic intermittent titration technique (GITT) and in situ X-ray diffraction (XRD) experiments are performed at very low rates in various voltage ranges (3.8–4.3 V,). On the "4.2–4.3 V" plateau the R2 phase is transformed simultaneously in R3, R3 with H4 stacking faults and H4. As the charge proceeds above 4.17 V cell polarization increases, hindering Li deintercalation. In discharge, such polarization decreases immediately. Upon cycling, the polarization increases at each charge above 4.17 V. In discharge, the capacity and d*Q*/d*V* features below 4.1 V remain constant and unaffected, suggesting that the bulk of the material do not undergo significant structural defect. This study shows that the change in polarization results from the electrochemical behavior of the grain surface having very low conductivity above 4.17 V and high conductivity below this threshold. This new approach can explain the behavior observed with dopants like tungsten.

1. Introduction

The electrochemical behavior of $LiNiO_2$, discovered by Dahn in 1990,[1–3] led to intensive researches on this material[4–12] and on lithium-nickel-based layered oxides $Li(Ni,M)O_2$ (M = Co, Mn, Al, Fe, Mg).[13–20] $LiNiO_2$ is very interesting from the electrochemical point of view, but its low thermal stability in the highly deintercalated state led to unsafe batteries.[21] Ohzuku showed that partial aluminum substitution improves the thermal stability of this material in the charged state.[22] Ukyo and Ikuhara made a systematic study of the Li(Ni,Co,Al) O_2 system and proposed NCA composition,[23–24] which is now currently used in electric vehicles. By high-resolution transmission electron microscopy, they showed the irreversible formation of a rocksalt layer on the particle surface at high voltage due to a reaction with the electrolyte.[25]

In 1999, Ohzuku showed the very interesting behavior of the $Li(Ni_{1/3}Mn_{1/3}Co_{1/3})O_2$ phase, which also presents an improved thermal stability and good electrochemical performance.[26] This opened the way to the NMC family, which is now the most commercially applied positive electrode material for electric vehicles.[27–32] For all layered positive electrode materials, a large anisotropic unit cell contraction was observed as the charge proceeded beyond 70% of de-intercalated lithium ions. Such local strains and resulting stress lead to the formation of cracks and fractures of secondaries and even primary particles, which lead to an increase of the cell resistance and reactions with the liquid electrolyte yielding to metal dissolution and ultimately rocksalt surface collapse.[33] Various coating, doping, and NMC-concentration gradient technologies were developed to limit the reactivity with the electrolyte at high voltage and ultimately to avoid the formation of the rocksalt-type structure at the surface of the particles.[33–47]

E. Bautista Quisbert, M. Guignard, C. Delmas
CNRS Université de Bordeaux
Bordeaux INP
ICMCB UMR 5026, 87
Avenue du Dr. Albert Schweitzer, Pessac Cedex, Pessac 33608, France
E-mail: edgarbautistaquisbert@gmail.com;
Marie.Guignard@icmcb.cnrs.fr; delmas@icmcb-bordeaux.cnrs.fr

The ORCID identification number(s) for the author(s) of this article can be found under https://doi.org/10.1002/smll.202300616.

DOI: 10.1002/smll.202300616

F. Fauth
CELLS ALBA Synchrotron
Barcelona E-08290, Spain
E-mail: ffauth@cells.es

A. M. Abakumov
Center for Energy Science and Technology
Skolkovo Institute of Science and Technology
Nobel str. 3, Moscow 121205, Russia
E-mail: a.abakumov@skoltech.ru

M. Blangero
Umicore rechargeable battery materials
27, 3gongdan 2-ro, Seobuk-gu, Cheonan-si, Chungnam 31093, South Korea
E-mail: Maxime.Blangero@ap.umicore.com

Further capacity increase in the NMC ternary diagram while keeping the application voltage in a moderate range like 4.2–4.3 V per graphite was best achieved by increasing the nickel content, reaching up to 90% in recent years. Positive electrode materials with such large Ni content present two main challenges. First, a significant part of the capacity is lost at the first cycle,[48] which is larger than that required to balance the capacity of the negative electrode. Second, when the cell is cycled at increasingly higher voltages above 4.2 – 4.3 V (vs Li^+/Li), the cell capacity retention rapidly degraded.[49–55] Among the various hypothesis that were proposed, the formation of rocksalt layer on the particle surface is well accepted. Moreover, even if some doping (with Zr, Nb, W) leads to significant improvements in the cycling properties the real mechanism is not really understood.

$LiNiO_2$ was adopted as a simpler model system to further investigate the structural phenomenon, kinetic limitations, and thermodynamic phase diagrams occurring at high voltage. Many studies of the electrochemical behavior of $LiNiO_2$ were reported in the literature.[56–59] Upon lithium deintercalation from $LiNiO_2$ (designed by R0: R-3m) several phases are successively formed: M1 (Monoclinic C2/m), R2 (R-3m), R3 (R-3m) and H4 (Hexagonal P-3m1). The R0, M1, R2, and R3 phases have the O3 type oxygen packing, their structures differ only by the lithium–vacancy ordering in the interslab space. Therefore, the phase transitions do not require much energy. The formation of the H4 (fully deintercalated NiO_2 phase O1 type packing) requires slab glidings and a larger activation energy. Nevertheless, as the NiO_2 slabs are preserved the reaction is fully reversible.[60–61] Several galvanostatic intermittent titration technique (GITT) experiments have been reported to determine the overall structural evolution upon cycling and its reversibility. Nevertheless, no very detailed electrochemical study has been performed in the high voltage range.

In this work, our goal was to investigate the effect of cycling above 4.15 V on the overall cell capacity when cycling over several voltage ranges. First, we synthesize a large batch of $LiNiO_2$ to perform all our experiments. The cells were cycled at low rate, in potentiostatic mode or in GITT mode with a long relaxation time to follow the capacity loss and the changes in cell polarization. In situ powder X-ray diffraction (XRD) experiments in GITT conditions were also performed on the 4.2-4.3 V plateau. This plateau has long been attributed to the biphasic domain between the R2 and R3 phases.[20] High-resolution transmission electron microscopy was also performed to follow the structural changes at the local scale. These experiments show that: i) the behavior on the high voltage plateau is more complicated than previously reported, ii) the irreversible overall capacity loss only occurs on this plateau due to the continuous polarization build-up at each charge above 4.15 V. At the very beginning of the discharge, the instantaneous decrease of the cell polarization shows that the electrochemical behavior of the rocksalt type thin layer plays a major role.

2. Results

2.1. High Voltage Cycling

$LiNiO_2$ was characterized by XRD to check the stoichiometry and the nickel distribution. Rietveld refinement using the Li atomic isotropic displacement parameter (B_{ISO}) method, that we proposed more than 25 years ago,[11] leads to the following cationic distribution $Li_{0.985}Ni_{0.015}NiO_2$ (Figure S1), (Table S1, Supporting Information).

A $Li//Li_xNiO_2$ battery was charged at the C/20 rate until 4.15 V and then the voltage was maintained until the current was close to zero in order to have a very homogenous state. In a second step, the charge was continued in GITT mode at very low C/100 rate corresponding to an increment of $\Delta x = 0.01$, followed by a fixed 10 h relaxation time on the 4.15–4.3 V range. In a third step, the cell was discharged in similar GITT conditions until 4.15 V. In a final step, the cell was discharged galvanostatically at C/20 to 3.0 V. The general shape of the cycling curve corresponds to the classical one, with an irreversible capacity loss of ≈14% of the first charge capacity. The GITT experiment shows that the cell voltage of the high voltage plateau above 4.15 V increases slightly, then rapidly (**Figure 1**).

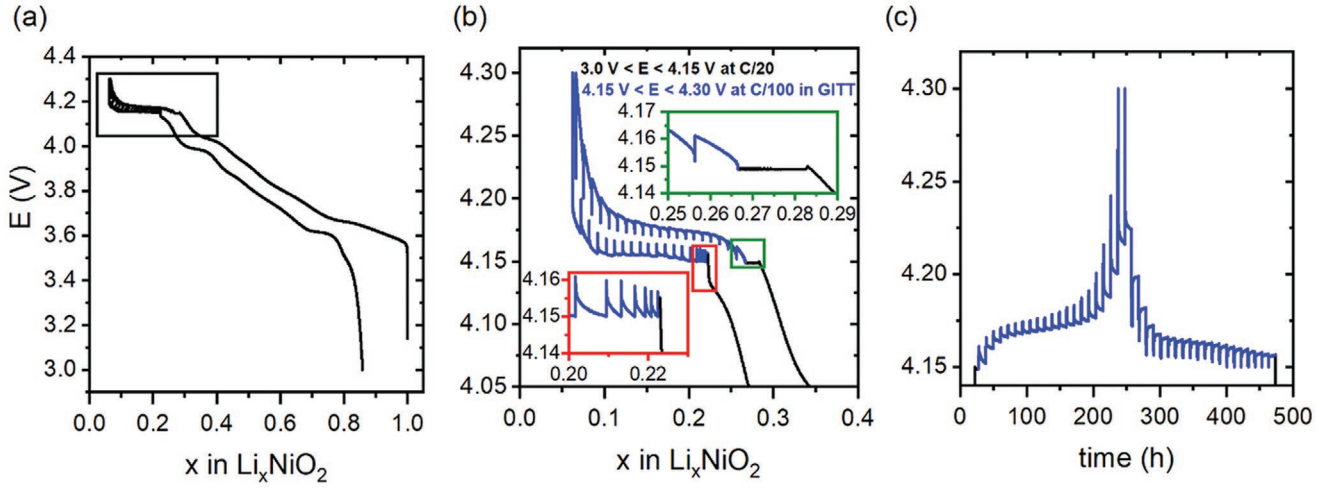

Figure 1. a) E versus *x* curve for a $Li//Li_xNiO_2$ cell charged galvanostatically at C/20 up to 4.15 V. At this voltage, the cell was floated until the current reached zero to ensure homogeneity. Afterward, the cell was charged/discharged between 4.15 V and 4.3 V in GITT mode at C/100. Finally, the cell was discharged, at C/20, to 3.0 V. b) Enlargement of the GITT part shown in the black rectangle in (a). The same part of this cycle versus time c) shows that the equilibrium is never reached.

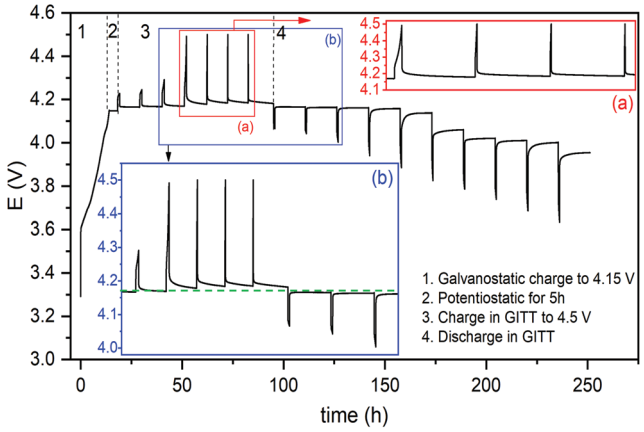

Figure 2. E versus time curve for the charge-discharge of Li//Li_xNiO_2 in an in situ cell for XRD at C/20. **(1)** charge up to 4.15 V in galvanostatic mode, **(2)** potentiostatic at 4.15 V for 5 hours, **(3)** charge in GITT mode (Δx = 0.05 + 10-hour relaxation), **(4)** discharge in GITT mode (Δx = 0.03 + 15-hour relaxation). The red inset a) shows the negligible Li deintercalation in the end of charge and the blue inset b) shows the continuous variation of the cell voltage after each charge/discharge pulse.

Enlargements of the curves versus the lithium content (x) and the time (Figure 1b,c) show that there is a continuous voltage change after each relaxation, which is not expected for a two-phase domain. Moreover, even after 10 h relaxation (after charge or discharge) at C/100 the equilibrium is never reached that indicates a slow intercalation-deintercalation kinetic (zoom Figure 1b).

These results show that the battery was in fact far from the equilibrium after each GITT step. Above $E \approx 4.17$ V, at each charge step, there is an increase in the polarization. Once the cell voltage reaches 4.3 V, the experiment continues in discharge with a very similar behavior. This shows that there is the formation of an insulating phase above 4.17 V. During the Li reintercalation, there is a rapid decrease of the cell resistance which suggests a reversible mechanism. Nevertheless, there is a shift in the x values, which might result from a reaction with the electrolyte because the cell was maintained at high voltage during a very long time. In summary, this experiment shows that the transition from R2 to R3 is not a classical two-phase domain. Moreover, one has to notice that the increase in polarization observed during the charge on the pseudo-plateau is reversible in discharge. This point will be discussed in the last part of this publication.

2.2. In Situ XRD – GIIT Characterization

In this section, we combined galvanostatic charge in GITT mode and in situ XRD measurements in a home-made electrochemical cell. As shown in the cycling experiment reported in **Figure 2**, the electrochemical study starts by a galvanostatic charge until 4.15 V (domain 1). Then, the cell was kept in potentiostatic mode for 5 h (domain 2). In the next step, the cell was charged in GITT mode (Δx = 0.05, 10 h relaxation) up to 4.5 V. All charges were performed at C/20. XRD patterns were collected at the very end of each relaxation in the 17–22° ($2\theta_{Cu}$) range, where the diffraction peaks related to the interslab distance are expected. As shown in domain 3, the cell voltage increases very rapidly to reach 4.5 V. The zoom (a) shows that only a very small amount of Li ions is deintercalated when the cell voltage increases rapidly to 4.5 V. This indicates that the deintercalation process is very difficult as already shown in Figure 1. In the second part of the study, in domain 4, the cell was discharged to 3.95 V.

As the R2 – R3 transition is considered as a biphasic one, a voltage plateau was expected at ≈4.15 V. This experiment shows clearly that the equilibrium was never reached during the relaxation after the charge above 4.15 V (insert (b)). The strong increase in voltage during the charge step shows that the cell resistance increases at the phase transition. Moreover, there is a small increase in the relaxed voltage at each charge step and a small decrease in the discharge one. As previously mentioned, this new experiment suggests that another mechanism more complicated than a classical two-phase domain is involved. One has also to notice that the cell polarization decreases at the charge/discharge transition (insert b). This point will be further discussed.

The changes in the XRD patterns confirm this behavior. Upon charge (**Figure 3**a), the R2 phase disappears without any

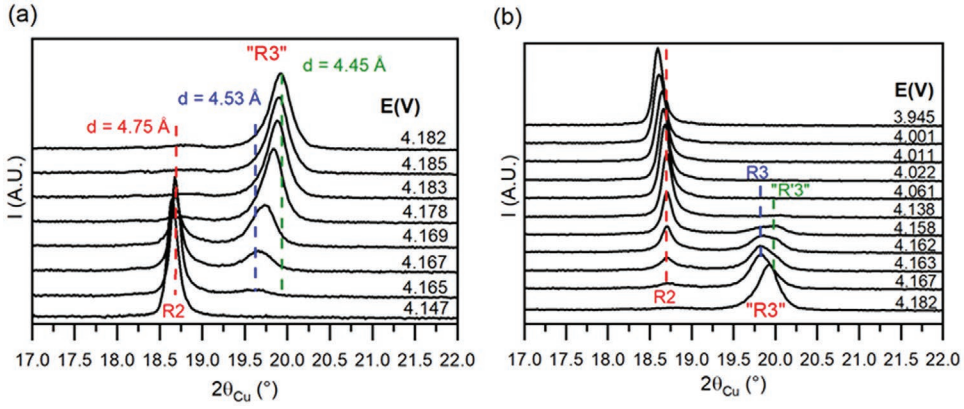

Figure 3. a) XRD patterns were recorded during the charge between 4.15 and 4.5 V and b) discharge between 4.18 V and 3.95 V, in GITT mode. The cell voltages E(V) at the end of the relaxation are reported. The dashed red line shows the position of the *003* reflection of the R2 phase, with a fixed d-spacing. For the "R3" phase, marked with the blue and green dashed lines, the d-spacing changes during charge (a) and during discharge (b). The discharge shows that the "R3" phase is as a combination of two phases.

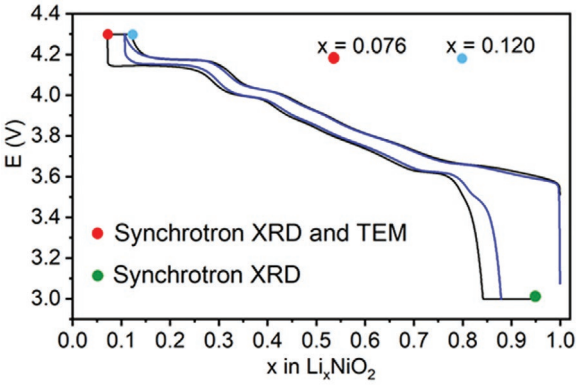

Figure 4. *E* versus *x* curves for Li//Li_xNiO_2 cells. In black, it is shown one of four curves for the galvanostatic charge to 4.3 V followed by a potentiostatic step at this voltage for 6 days, then the discharge to 3.0 V followed by a potentiostatic step till the current was close to 0 mA. The electrode material of two cells were recovered in charge (red point) and two others at the end of discharge (green point). The curve (blue) for the galvanostatic classical charge and discharge between 3.0 and 4.3 V is given for comparison.

change in the peak position, as expected, while the position of the "R3" peak is continuously shifted to higher 2θ values. Moreover, this diffraction line is considerably broadened versus the R2 one. This suggests the existence of a distribution of interslab distances. The ideal NiO_2 phase (H4) exhibits an O1 oxygen packing and a smaller interslab distance (a = 2.814(6) Å and c = 4.346(2) Å).[60] It was shown in the literature the occurrence of stacking faults at the end of the lithium deintercalation from $LiNiO_2$ that leads to a broadening of the diffraction lines associated to their displacement.[57] The presence of an increasing number of O1 slabs, with a smaller interslab distance, leads to displacement of the diffraction line to larger 2θ values.

After observing the changes in the XRD patterns during charge, the discharge process was performed in GITT mode. The XRD patterns, shown in Figure 3b, reveal that the shift of the "R3" peak is due to the apparition of another peak. The difference in the XRD patterns recorded during charge and discharge reveals that the "R3" diffraction line is a combination of two peaks that may correspond to R3 domains (O3) (larger interslab distance, i.e., lower 2θ-values) and stacking faulted "R"3" domains (O3-O1) (shorter interslab distance, i.e., larger 2θ-values) that can be distinguished due to different kinetics during the Li reintercalation. One can assume that the Li reintercalation is more difficult in the O1 interslab space, which is shorter than in the O3 type one. Moreover and according to lattice invariant shear symmetry constraints, this O1 to O3 transition needed to transform back to the R2 phase, requires a slab gliding which increases the activation energy. This may explain why the diffraction peak associated to "R"3" domains at higher 2θ-values disappears last.

The change in polarization at the transition between charge to discharge suggests the formation of a material with a very low conductivity (electronic or ionic) at each charge above 4.15 V and the formation of a conductive material as soon as lithium is reintercalated in the material. This agrees with the results observed during the GITT discharge shown in Figure 1c.

2.3. Structural Characterization

To gain more information about the material obtained at 4.3 V, Li//Li_xNiO_2 cells were charged (one charge or one cycle) to obtain materials for structural characterization. Four cells were galvanostatically charged (C/20) to 4.3 V in a first step, then potentiostatically at 4.3 V until the current became close to 0 mA (144 h). Besides, two of them were discharged to 3.0 V. **Figure 4** gives the cell voltage variation versus the lithium amount (black curve) in comparison to that of a cell without the potentiostatic step at 4.3 V (blue curve). The difference in capacity at high voltage shows that the polarization (blue curve) prevents for a full electrochemical deintercalation. In discharge, the capacity on the high voltage plateau of the overcharged cell (black curve) is higher than that of the other battery. This comparison shows that the cell polarization above 4.2 V limits the charge in normal cycling conditions. Only 0.044 Li, per formula unit, was deintercalated during the 144 h potentiostatic charge at 4.3 V. In Figure S2, Supporting Information, this experiment is given as a function of time to show the current changes during the potentiostatic steps. At the very beginning of the potentiostatic step at 4.3 V, the current dropped instantaneously, then slowly decreased until the end of the step. Even after the very long potentiostatic charge the equilibrium was never obtained (zoom in Figure S2, Supporting Information). One can assume that the lithium deintercalation continued to occur with the formation of the H4 phase. A continuous reaction with the electrolyte must also be considered as shown by the very low, but never equal to 0 mA, constant current.

All cells were dismantled at the end of the charge (or discharge) to characterize the recovered active material by synchrotron XRD and high resolution TEM. The Synchrotron-XRD (S-XRD) patterns (**Figure 5**a) of pristine $LiNiO_2$ (blue curve) and of the material recovered after one cycle (black curve), which are indexed in the R-3m space group, show the complete reversibility of the intercalation reaction. As shown in the panels (5b) to (e), the diffraction lines, of both materials, are very similar. Moreover, there is a slight broadening of the diffraction peaks that shows that there is no structural defects neither major change in the coherent grain size after a full cycle of charge and discharge. Rietveld refinement of the S-XRD pattern recovered after the full discharge is given in Figure S3, Supporting Information. The cell parameters (**Table 1**) and the amount of Ni in the lithium site (Table S2, Supporting Information) are very similar to those of the pristine material (Table S1, Supporting Information). The very small increase in the $c_{hex.}$ parameter results from the difference in Li content (0.940 mole of Li in the Li_xNiO_2 phase obtained at the end of the discharge compare to 0.985 mole of Li in the pristine phase). These results show that the structure is maintained and there is no nickel migration from the NiO_2 slab to the interslab space. The large Crystal Field Stabilization Energy CFSE) of Ni^{4+} (t_{2g}^6 LS) in octahedral site and the very low one in tetrahedral site ($e^3\,t_2^3$) makes difficult the nickel migration to the tetrahedral sites in the bulk of the O3 type phase. This behavior would be very different from the formation of rocksalt type phase at the surface of the particles which is due to the reaction with the electrolyte and leads to an oxygen loss. In a recent paper, the migration of nickel to the tetrahedral sites was assumed on

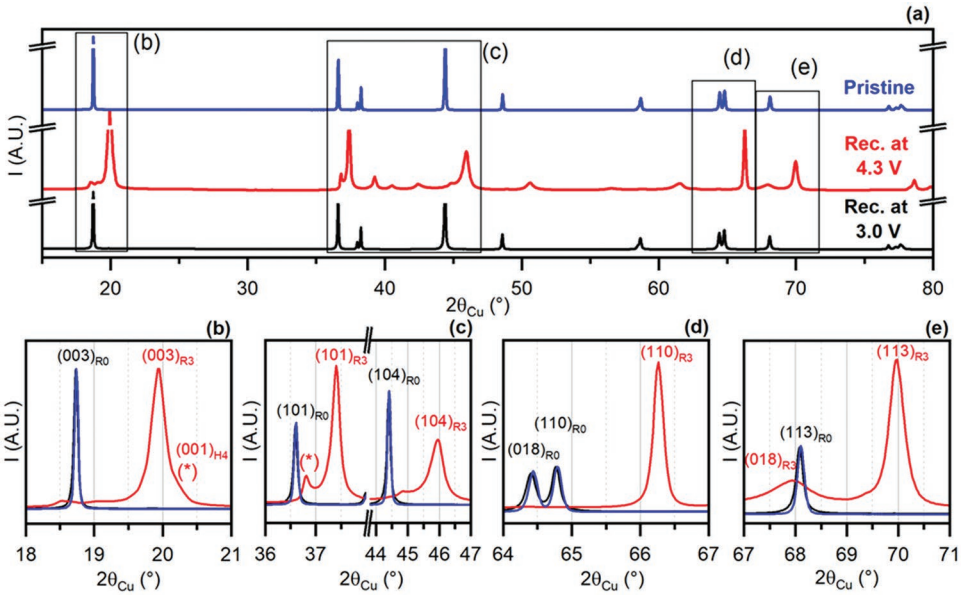

Figure 5. S-XRD patterns (converted to Cu wavelength) for different Li_xNiO_2 phases: pristine (in blue, *R-3m*, a = 2.875 Å, c = 14.187 Å), recovered at 4.3 V after potentiostatic for 144 hours (in red, *R-3m*, a = 2.812 Å, c = 13.340 Å) and recovered at 3.0 V after one-cycle (in black, *R-3m*, a = 2.876 Å, c = 14.199 Å) (Panel (a)). Panels (b) through (e) are enlargements in selected 2θ ranges to show the peak broadening in the sample recovered at 4.3 V. The pattern in red displays some stars for peaks characteristic of the H4 phase present at 4.3 V.

the R2-R3 plateau.[62] In this study, there is no evidence of this migration which will be discussed in a following paper.

For the material recovered at 4.3 V, there is an important shift of the diffraction lines due to the change in cell parameters. Most of the diffraction peaks (blue line) can be indexed in the R-3m space group (O3 oxygen packing). The cell parameters (a = 2.812Å, c = 13.340 Å) are in agreement with the literature for the R3 phase.[63] (**Figure 6**a). The remaining diffraction peaks (green lines), with very weak intensity, can be indexed in the P-3m1 space group, characteristic of the H4 type phase (O1 oxygen packing) (Figure 6b). Table 1 gives a summary of the lattice parameters of all the involved phases.

The O3 type phase exhibits an AB CA BC AB oxygen packing along the c direction of the hexagonal lattice while the O1 one exhibits an AB AB one. When a slab gliding occurs in the lattice, there is formation of a stacking fault. Inside the O3 packing, there is local AB AB domains which leads to a diffraction line broadenning. Therefore, there is a significant broadening of some diffraction lines which shows the occurrence of stacking faults in the R3 phase formed after the potentiostatic charge to 4.3 V. As usual in layered oxides, the line broadening is very sensitive to the *hkl* values. The d-spacing of the 003 diffraction line (R3) is strongly enlarged due to the smaller interslab distance in O1 ($c_{hex.}$ = 4.365 Å) versus O3 ($c_{hex.}/3$ = 4.447 Å) (Figure 5a). The same tendency is illustrated by comparing the 018 lines broadening of the pristine and that of the material recovered at 4.3 V (Figure 5d,e). On the opposite, the 110 one is less affected (Figure 5d) as there is almost no change in the $a_{hex.}$ parameters of R3 and H4 phases.

In conclusion of this part, the S-XRD study of the pristine and the material recovered after one cycle, which are indexed in the R-3m space group, shows the complete reversibility of the reaction. Moreover, there is no broadening of the diffraction lines showing that the stacking faults have disappeared during the Li reintercalation. These results also show that there is no nickel migration from the NiO_2 slab to the interslab space.

Table 1. Summary of structural data corresponding for the pristine material and for the materials recovered after the charge/discharge of Li//Li_xNiO_2 batteries at different conditions.

Name	Composition	Space group	a_{hex} [Å]	c_{hex} [Å]
Pristine	$Li_{0.985}Ni_{1.015}O_2$	R -3 m	2.875	14.187
Recovered at 3.0 V after 1 cycle to 4.3 V	$Li_{0.940}Ni_{1.015}O_2$	R -3 m	2.876	14.199
Recovered after 1 charge to 4.3 V O3 indexation (R3)	$Li_{0.076}Ni_{1.015}O_2$	R -3 m	2.812	13.340
Recovered after 1 charge to 4.3 V O1 indexation (H4)	$Li_{0.076}Ni_{1.015}O_2$	P-3m1	2.812	4.365

2.4. High-Resolution Transmission Electron Microscopy

High resolution transmission electron microscopy was performed on the sample recovered from the battery charged to 4.3 V. Several images (HAADF-STEM) are shown in **Figure 7** where the nickel ion layers are clearly visible. In the [010] zone axis, the nickel ion packing is clearly seen Figure 7a). Studying how two successive nickel layers are stacked allows determining the oxygen packing type (O3 or O1). In the O3-type oxygen packing, nickel layers are shifted from each other in the (ab) plane, while for the O1 type packing, nickel layers are stacked on top of each other with no shift. Figure S4a, Supporting Information, represents the Ni ions packing (blue line) in an

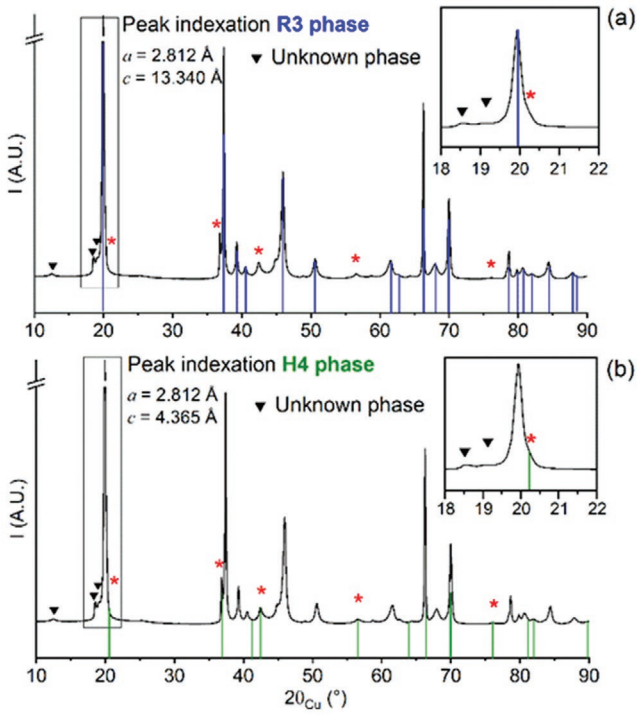

Figure 6. S-XRD pattern (converted to Cu wavelength) for an electrode recovered at 4.3 V. a) Peak indexation done for the R3 phase (blue lines), b) peak indexation done for the H4 phase (green lines). The red stars show the peaks characteristic of the H4 phase and the black arrows show peaks from an unknown phase.

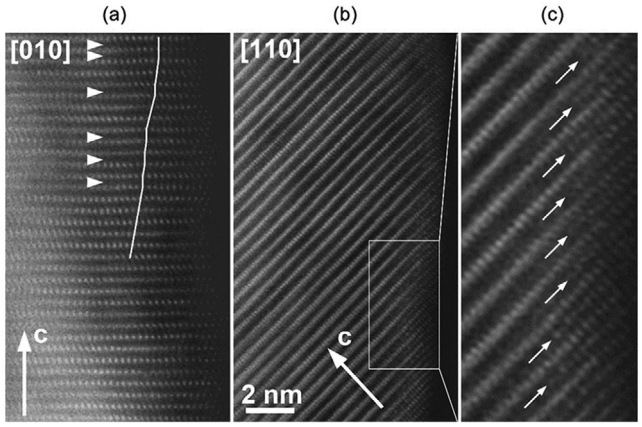

Figure 7. [010] and [110] HAADF-STEM images of the Li_xNiO_2 phase recovered from the battery charged to 4.3 V. a) The stacking sequence of the (NiO_2) slabs is traced with the white line in the [010] image. O3 type packing is indicated by the slightly sloping line, while the O1-type interslabs space are marked with arrowheads. b,c) show the presence of nickel in the lithium layer at the extreme surface of the particle (marked with arrows in (c)).

ideal O3 type structure (continuous shift) and in a material with an O1 stacking fault (no shift of the Ni layer) in the O3 structure (Figure S4b, Supporting Information). In the HAADF-STEM image (Figure 7), O1-type stacking faults (indicated by the arrows) appear within the O3-type matrix which remains largely predominant. The driving force of the O3 to O1 transition results from the competition between the stabilization of the O3 type structure due to the presence of lithium ions in octahedral sites between the NiO_2 slabs and the oxygen-oxygen repulsion, when almost all lithium ions are removed, which destabilizes the O3 type structure. At the end of the Li deintercalation, there is tendency to form locally O1-type domains by slab gliding which decreases the oxygen orbital overlapping (see the scheme in Figure S5, Supporting Information).

[110] HAADF-STEM image in Figure 7b shows the presence of nickel in the lithium layer on the extreme surface of the particle. This confirms that at 4.3 V there is a minor oxygen loss leading to the formation of a rocksalt like material due to the reaction with the liquid electrolyte. The rocksalt type layer is very thin (2 nm) compared to the size of the pristine $LiNiO_2$ particle (200 – 300 nm).

In conclusion, these results confirm the S-XRD ones: stacking faults occur in the Li_xNiO_2 phase when the battery is charged to high voltage and appearance of O1 type structure domain which represent traces of the H4 phase. The presence of only a small amount of O1 packing after a very long potentiostatic charge (144 h) gives evidence that the kinetics of the deintercalation is very low. This effect can result: i) from the difficulty for slab glidings in the O3 structure to happen and ii) from the low conductivity of the rocksalt layer formed at the particle surface, which limits the Li deintercalation.

2.5. Relation Between the Polarization at High Voltage and the Capacity Loss

In the previous part, we have shown that there is the formation of H4 domains and a strong increase of the polarization of the cell when the batteries $Li//Li_xNiO_2$ are charged above 4.15 V. The XRD study shows that the reaction is fully reversible from the structural point of view. To better understand the origin of the increase in polarization at high voltage, new experiments were realized to compare the cycling behavior with an upper voltage limitation of 4.3 V, 4.2 V and 4.1 V. **Figure 8** shows the galvanostatic cycling in the 3.0–4.3 V range. As shown in the zoom of Figure 8a, the polarization in charge increases rapidly upon cycling leading to a capacity decrease on the high voltage plateau while the capacity remains almost constant in the first part of the charge. This behavior appears clearly in the voltage versus capacity curves (Figure 8b). To compare the capacity changes above and below 4.15 V, the voltage versus capacity curves were shifted to superpose all the curves, on the first discharge one, at 3.7 V (zoom in Figure 8b and Figure S6, Supporting Information). Upon cycling, the capacity below 4.15 V is almost constant while that above 4.15 V decreases very rapidly. As shown in the zoom, the voltage decreases rapidly at the beginning of the discharge, then increases again. This shows that the polarization observed during successive charges decreases at each discharge, but increases continuously at each charge to 4.3 V. A similar behavior, attributed to bulk fatigue induced by surface reconstruction was recently reported.[55] The superposition of the curves shows that the capacity is fully maintained below 4.0 V. The same behavior is observed when the voltage is limited to 4.2 V (Figure S7, Supporting Information)

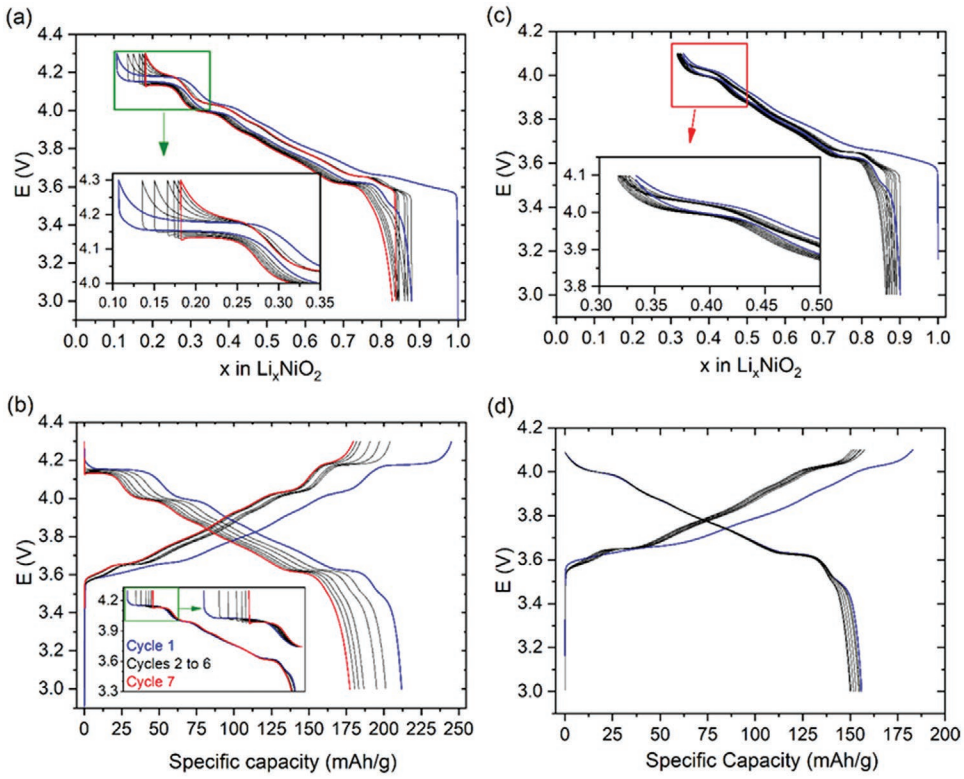

Figure 8. *E* versus *x* and *E* versus *Q* curves for the galvanostatic charge/discharge for a Li//Li_xNiO_2 cell between: a,b) 3.0 and 4.3 V and c,d) 3.0 and 4.15 V at C/20. The insets in (a) and (c) zoom at the end of the charge and the beginning of the discharge and the inset in (b) shows the discharge capacity shifted to superpose the discharge curves at 3.7 V.

with a smaller high voltage polarization either in charge and in discharge.

For comparison, batteries were cycled at the same rate C/20 up to 4.1 V. As shown in Figure 8c,d there is no increase of the polarization at the end of charge. There is only a small capacity shift at high voltage and a larger one at the end of the discharge. In Figure 8d, the curves show that the capacity is maintained in the 3.6 – 4.1 V range. The problem concerning the capacity loss observed at low voltage (below 3.5 V) is not yet understood. It is the purpose of an ongoing research.

To study in more details the polarization change at high voltage, cells were cycled 10 times in the 3.8 – 4.3 V range followed by a discharge down to 3.0 V as shown in **Figure 9**. The capacity on the high voltage pseudo-plateau decreased continuously upon cycling while it is maintained in the 3.8-4.1 V range (Figure 9a). There is an increase, at each cycle, of the polarization in charge above 4.17 V and in the first part of the discharge (Figure 9b). The polarization is strongly reduced when the cell voltage is less than $E \approx 4.12$ V. The zoom of the curve during the charge shows the rapid increase of the cell voltage above 4.15 V. When 4.3 V is reached, the cell is discharged. In the first 30 s (the duration between two data recording) the voltage goes down to 4.12 V (Figure 9c). During this period, 0.0004 lithium ions per Li_xNiO_2 formula are reintercalated. Then the voltage increases slightly during few minutes and then drops. Such a small reintercalation amount, which induces a 0.18 V drop, cannot result from a normal reintercalation process. The voltage increase during a discharge, forbidden from the thermodynamic point of view, shows that there is a change in the kinetics responsible for the shape of the curve. This very small amount of reintercalated lithium during the voltage drop cannot induce a significant change in the kinetics properties of the bulk of the Li_xNiO_2 particles. Therefore, one can assume that it is the surface layer which is involved. Therefore, the "rocksalt layer" and/or the cathode-electrolyte interphase layer must be considered in this peculiar process. In our knowledge such behavior was never reported in the literature even at very high voltage. Between these two possibilities, we make the hypothesis that it is the rocksalt layer, which is involved. The re-intercalation of 0.0004 lithium (per Li_xNiO_2) would lead to a large change in composition of the thin rocksalt layer and a change in the kinetics of the lithium transfer. New experiments will be done, in our future research, to try to confirm this hypothesis.

A similar experiment was realized in the 3.8 – 4.15 V range for 10 cycles followed by a discharge to 3.0 V. In this voltage range, there is no change in the cell polarization and no capacity loss (Figures S8 and S9, Supporting Information).The irreversible capacity after a full cycle (≈17%) is equal to the classic one at the first cycle. These results show that high polarization occurring on the 4.2–4.3 V pseudo plateau is disconnected from the behavior below the plateau (no polarization).

In a new experiments the upper voltage limit was alternated: 4.3 V then 4.15 V then 4.3 V (**Figure 10**). In the first step (black curve), there is a continuous increase of the polarization above 4.15 V. Then no change in the second step (red curve) where the

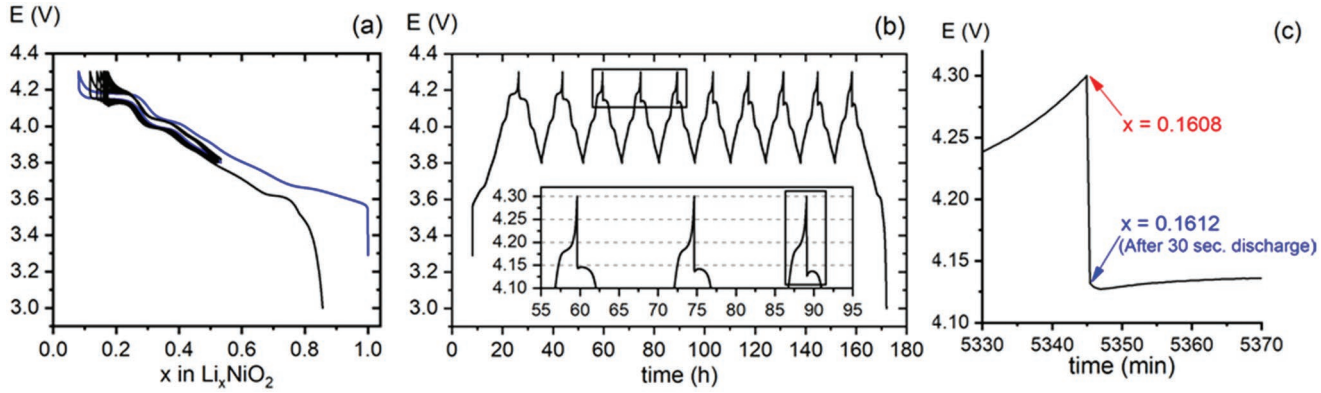

Figure 9. a) Potential (*E*) versus Li content (*x*), versus time (*t*) for the cycling between 3.8 V and 4.3 V for Li//LixNiO2 cell at C/20. The zoom of cycles 3–5 in Figure b) emphasizes the increasing polarization in charge at each cycle, which decreases upon discharge on the 4.12-4.15 V pseudo plateau. c) The 5th cycle has been zoomed and the *x*-axis changed to minutes.

voltage was limited to 4.15 V. The third step (blue curve) is the continuation of that of the 5th cycle (Figure 10a). On Figure 10b the 3th, 4th, and 5th cycling curves of the battery cycled to 4.3 V is superimposed to the 6th, 7th, and 8th cycle where the charge was limited to 4.15 V. The comparison shows that the capacity and the shape of the curves are identical below 4.15 V.

An experiment made to 4.2 V then 4.15 V then 4.2 V range (Figure S10, Supporting Information) shows the same tendency with a reduced polarization due to the lower voltage limit. These results confirms that 4.15 V is a critical value for the reversibility in the cycling of the Li_XNiO_2 positive electrode.

2.6. General Discussion

All these results point to 4.15 V/Li as the voltage limit to prevent polarization build-up at high voltage. As previously mentioned we make the hypothesis, not yet confirmed, that it is the rocksalt surface layer, which is involved in this mechanism and not the cathode-electrolyte interphase layer. This phenomenon is mainly due to the formation of the rocksalt type layer, on the surface of the primary particles, related to oxygen evolution (reaction with the electrolyte). In a recent publication it was proposed that the capacity loss results from the high interfacial lattice strain between the reconstructed surface and the bulk layered structure.[55] The reversibility of the polarization suggests that there is a dramatic change in the conductivity (ionic and/or electronic) of the rocksalt type layer linked to the cell voltage.

The transformation of Li_xNiO_2 ($x \approx 0.15$) into rocksalt type phase at the particle surface is well-known, but its effect on the intercalation kinetic versus the cell voltage has never been considered. The general formula of the rocksalt type phase is "Li_zNi_tO" with $z + t \leq 1$. The oxidation state of nickel is $(2 - z)/t$. At each cycle, the lithium content of the rocksalt layer is continuously modified. Moreover, at each charge above 4.15 V, the amount of Ni in this phase slightly increases due to the reaction with the electrolyte. One has to consider the rocksalt phase as an active material, which exhibits its own electrochemical curve. The Li intercalation /deintercalation from Li_zNi_tO rocksalt leads to a strong change in its conductivity. Below 4.15 V, the conductivity of the rocksalt thin layer is high, there is no significant effect on the cycling of the Li_xNiO_2 phase within the bulk of the particle. Above 4.15 V, its low conductivity lead to a high polarization, which makes difficult the lithium deintercalation from the Li_xNiO_2 phase. (**Figure 11**). Moreover, at each charge above 4.15 V the reaction with the electrolyte leads: i) to an increase of the Ni/O ratio in the rocksalt type layer, ii) and to an increase in its thickness. Both effects lead to an increase of the cell polarization at high voltage, which limits the capacity obtained for the 4.2–4.3 V pseudo plateau. Other parameters have also to be considered: the strong decrease in the interslab distance due to the transitions from the R2 to the R3 phase and to H4 phase lead to cracks in the particles and to an increase of the active surface area leading to the formation of more rocksalt type phase.

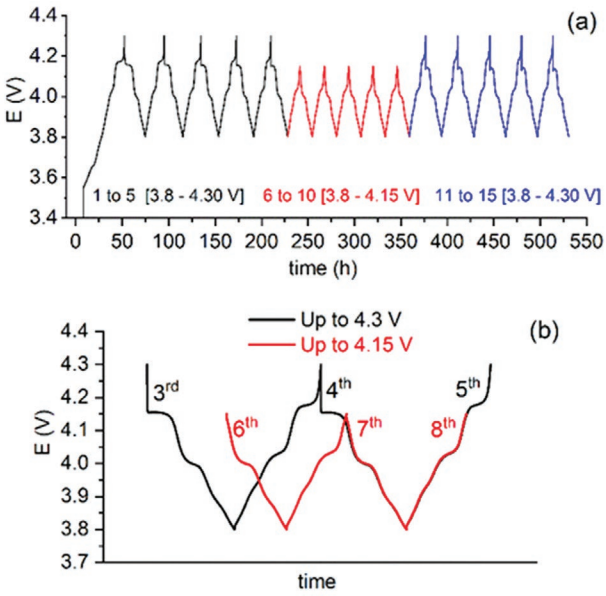

Figure 10. Charge/discharge at C/50 of a Li//$LiNiO_2$ cell charged up to 4.3 and 4.15 V; a) *E* versus time curve b) superposition of cycles 3, 4, and 5 (charge to 4.3 V) and cycles 6, 7, and 8 (charge to 4.15 V),

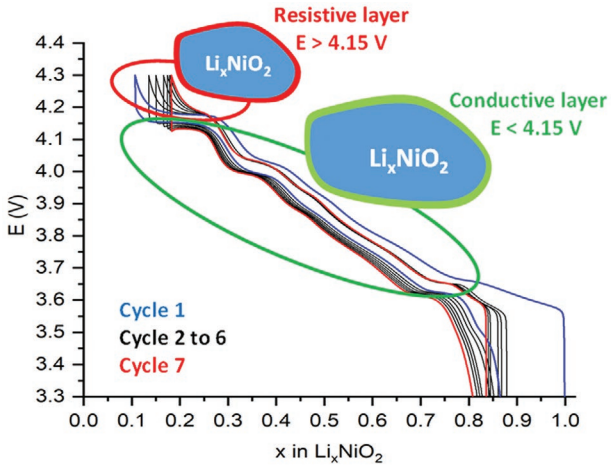

Figure 11. *E* versus *x* curves for the galvanostatic cycling of a Li//Li_xNiO_2 coin cell between 3.0 and 4.3 V at C/20. A particle surrounded by a thin surface layer is represented. Depending on the cell voltage, this thin layer is conductive or highly resistive.

3. Conclusion

This study shows that several phenomena occur simultaneously in the "4.2–4.3 V" voltage plateau: i) lithium deintercalation leading to the R2-R3 structural phase transition (O3 type is maintained) with change in the cell parameters; ii) simultaneous formation of H4 phase domains (O1 type packing) within the R3 structure (stacking faults), iii) irreversible formation of a rock-salt type phase (even at 4.2 V) leading to a strong polarization which disappears in discharge below 4.15 V. This change in the electrochemical behavior can result either from the rocksalt phase surface layer or from the cathode- electrolyte interphase. We made the hypothesis that the rocksalt phase surface layer is concerned. Nevertheless, this hypothesis must be experimentally confirmed.

Many researches attempted to stabilize the capacity at high voltage of Ni-rich layer oxides and NMC derivatives. An interesting approach was performed to monitor the chemistry (concentration gradient) and the structural orientation inside the primary particles. Most of the researches concern cationic substitution, to increase the capacity performances, and coating to try to prevent from the reaction with electrolyte. Some of them have led to promising results as it was shown recently by tungsten doping .[54] In these studies, significant improvements were obtained, but the effects of the electrochemical behavior of the rocksalt type layer have never been considered. One can assume that the change in composition at the surface of the particles, due to doping, monitors the electrochemical behavior of the rocksalt thin layer. The change in the structural parameters of the rocksalt layer at the voltage transition must be studied to see the influence of the lattice strains.[55] The results presented in this paper open a new approach to monitor the electrochemical behavior of the rocksalt type shell and manage its electrochemical properties, at high voltage, by cationic doping of the surface layer.

4. Experimental Section

$LiNiO_2$ was synthesized by direct solid-state synthesis from NiO and Li_2O. Several experiments were realized to optimize the Li/Ni ratio of the precursor and the temperature profile of the thermal treatment in order to have the lowest amount of nickel in the lithium sites. The best results were obtained with a 6% Li excess versus the nominal composition. Two thermal treatments (24 h at 665 °C and 24 h at 700 °C of the oxides mixture, with intermediate grinding) under oxygen flow lead to a material very close to the ideal stoichiometry. This material was characterized by powder XRD diffraction.

Powder XRD was performed using a PANalytical diffractometer and $Cu_{K\alpha}$ radiation (λ = 1.5418 Å). Phase identification was performed using XPert HighScore software, and structural refinement using the Rietveld method on TOPAS software. Data were collected with long acquisition in the 10–120° (2θ) range for Rietveld refinements.

Synchrotron-XRD (S-XRD) powder patterns have been registered on the BL04-MSPD beamline [*] of the ALBA synchrotron at either ≈20 keV or ≈30 keV (exact wavelength determined by measuring selected peaks of silicon SRM640d NIST standard). Data were collected in Debye Scherrer mode using the position-sensitive detector MYTHEN.[64]

Samples for transmission electron microscopy (TEM) were prepared by dispersing the powders in dry dimethyl carbonate in an agate mortar and depositing drops of suspension onto a carbon film supported by a copper grid. TEM samples were prepared in an Ar-filled glovebox. The samples were transferred to the microscope column with a Gatan vacuum transfer holder completely excluding contact with air and moisture. High angle annular dark field scanning transmission electron microscopy (HAADF-STEM) images were collected with a probe aberration-corrected Titan Themis Z electron microscope operated at 200 kV.

The electrochemical study was done either in coin cells or Swagelok-type cells, when a large amount of material is required for the structural characterization. Lithium is the negative electrode. Viledon and Celgard sheet are used as separators. The electrolyte is a 1 M solution of LiPF6 in a PC-EC mixture. In coin cells, the positive electrode is a mixture of $LiNiO_2$ (90%), carbon black (5%) and PVDF binder (5%). In Swagelok cells PTFE is used as a binder [($LiNiO_2$ (88%), Carbon black (10%), PTFE (2%)]. In situ XRD-battery cycling experiments were done in a homemade cell with a beryllium window on one side, using an Empyrean (Panalytical) diffractometer in reflection mode (Bragg–Brentano geometry), linked to a Biologic Battery cycler. In all cells, the positive electrode was calendered.

Supporting Information

Supporting Information is available from the Wiley Online Library or from the author.

Acknowledgements

The authors thank Region Nouvelle Aquitaine and Umicore company for financial support and fruitful discussions, CELLS-ALBA for provision of beamtime through BL04-MSPD in house program (proposal ID 2021035158), A.M.A. is grateful to the Russian Science Foundation for financial support (grant 20-13-00233). Access to TEM facilities was granted by the Advance Imaging Core Facility of Skoltech, Cathy Denage for experimental support and SEM image acquisition

Conflict of Interest

The authors declare no conflict of interest.

Data Availability Statement

The data that support the findings of this study are available from the corresponding author upon reasonable request.

Keywords

cell polarization, lithium nickel oxide, lithium-ion batteries, positive electrode materials

Received: February 23, 2023
Revised: March 13, 2023
Published online:

[1] J. Dahn, U. Von Sacken, C. Michal, *Solid State Ionics* **1990**, *44*, 87.
[2] J. Dahn, U. Von Sacken, M. X. Juskow, H. AL-Janaby, *J. Electrochem. Soc.* **1991**, *138*, 2207.
[3] W. Li, J. Riemers, J. Dahn, *Phys. Rev. B: Condens. Matter Mater. Phys.* **1992**, *45*, 3236.
[4] T. Ohzuku, A. Ueda, M. Nagayama, *J. Electrochem. Soc.* **1993**, *140*, 1862.
[5] T. Ohzuku, A. Ueda, M. Nagayama, Y. Iwakoshi, H. Komori, *Electrochem. Acta* **1993**, *38*, 1159.
[6] C. Delmas, *Mater. Sci. forum* **1994**, *152*, 131.
[7] R. Kanno, H. Kubo, Y. Kawamoto, T. Kamiyama, F. Izumi, Y. Takeda, M. Takano, *J. Sol. State Chem.* **1994**, *110*,216.
[8] A. Rougier, C. Delmas, A. V. Chadwick, *Solid State Commun.* **1995**, *94*, 123.
[9] M. Broussely, F. Perton, P. Biensan, J. M. Bodet, J. Labat, A. Lecerf, C. Delmas, A. Rougier, J. P. Pérès, *J. Power Sources* **1995**, *54*, 109.
[10] H. Arai, S. Okada, H. Ohtsuka, M. Ichimura, J. Yamaki, *Solid State Ion.* **1995**, *80*, 261.
[11] A. Rougier, P. Gravereau, C. Delmas, *J. Electrochem. Soc.* **1996**, *143*, 1168.
[12] J. P. Peres, C. Delmas, A. Rougier, M. Broussely, F. Perton, P. Biensan, P. Willmann, *J. Phys. Chem. Solids* **1996**, *57*, 1057.
[13] J. Dahn, R. Fong, U. Von Sacken, *Eur. Pat. Appl.* **1992**.
[14] C. Delmas, I. Saadoune, *Solid State Ionics* **1992**, *53*, 370.
[15] E. Rossen, C. Jones, J. Dahn, *Solid State Ionics* **1992**, *57*, 311.
[16] J. Reimers, E. Rossen, C. Jones, J. Dahn, *Solid State Ionics* **1993**, *61*, 335.
[17] T. Ohzuku, A. Ueda, M. Nagayama, Y. Iwakoshi, H. Komori, *Electrochem. Acta* **1993**, *38*, 1159.
[18] A. Rougier, Ph.D. thesis, Univ. Bordeaux, **1995**.
[19] T. Ohzuku, A. Ueda, M. Kouguchi, *J. Electrochem. Soc.* **1995**, *142*, 4033.
[20] C. Pouillerie, L. Croguennec, C. Delmas, *Solid State Ionics* **2000**, *132*, 15.
[21] J. Dahn, E. W. Fuller, M.-P. Obrovac, U. von Sacken, *Solid State Ionics* **1994**, *69*, 265.
[22] T. Ohzuku, T. Yanagawa, M. Kouguchi, A. Ueda, *J. Power Sources* **1997**, *68*, 131.
[23] S. Muto, Y. Sasano, K. Tatsumi, T. Sasaki, K. Horibuchi, Y. Takeuchi, Y. Ukyo, *J. Electrochem. Soc.* **2019**, *156*, A371.
[24] Y. Makimura, S. Zheng, Y. Ikuhara, Y. Ukyo, *J. Electrochem. Soc.* **2012**, *159*, A1070.
[25] S. Zheng, R. Huang, Y. Makimura, Y. Ukyo, C. Fisher, T. Hirayama, Y. Ikuhara, *J. Electrochem. Soc.* **2011**, *158*, A357.
[26] T. Ohzuku, Y. Makimura, *Chem. Lett.* **2001**, *30*, 642.
[27] Y. Koyama, I. Tanaka, H. Adachi, Y. Makimura, T. Ohzuku, *J. Power Sources* **2003**, *19*, 644.
[28] N. Yabuuchi, Y. Makimura, T. Ohzuku, *J. Electrochem. Soc.* **2007**, *154*, A314.
[29] N. Yabuuchi, Y. Koyama, N. Nakayama, T. Ohzuku, *J. Electrochem. Soc.* **2005**, *152*, A1434.
[30] F. Zhou, X. Zhao, J. Dahn, *J. Electrochem. Soc.* **2009**, *156*, A343.
[31] J. Zheng, W. Kan, A. Manthiram, *ACS Appl. Mater. Interfaces* **2015**, *7*, 6926.
[32] W. Li, X. Liu, H. Celio, P. Smith, A. Dolocan, M. Chi, A. Manthiram, *Adv. Energy Mater.* **2018**, *8*, 1703154.
[33] V. Meunier, M. De Souza, M. Morcrette, A. Grimaud, *J. Electrochem. Soc.* **2021**, *169*, 070506.
[34] S. Liu, X. Chen, J. Zhao, J. Su, C. Zhang, T. Huang, J. Wu, A.i. Yu, *J. Power Sources* **2018**, *374*, 149.
[35] Q. Ran, H. Zhao, Y. Hu, Q. Shen, W. Liu, J. Liu, X. Shu, M. Zhang, S. Liu, M. Tan, H. Li, X. Liu, *Electrochim. Acta* **2018**, *289*, 82.
[36] Y. Su, Y. Yang, L. Chen, Y. Lu, L. Bao, G. Chen, Z. Yang, Q. Zhang, J. Wang, R. Chen, S. Chen, F. Wu, *Electrochim. Acta* **2018**, *292*, 217.
[37] H. Ryu, K. Park, D. R. Yoon, A. Aishova, C. S. Yoon, Y. K. Sun, *Adv. Energy Mater.* **2019**, *9*, 1902698.
[38] X. Li, K. Zhang, M. Wang, Y. Liu, M. Qu, W. Zhao, J. Zheng, *Sustainable Energy Fuels* **2018**, *2*, 413.
[39] F. Schipper, H. Bouzaglo, M. Dixit, E. Erickson, T. Weigel, M. Talianker, J. Grinblat, L. Burstein, M. Schmidt, J. Lampert, C. Erk, B. Markovsky, D. Major, D. Aurbach, *Adv. Energy Mater.* **2018**, *8*, 1701682.
[40] D. Rathore, C. Geng, N. Zaker, I. Hamam, Y. Liu, P. Xiao, G. Botton, J. Dahn, C. Yang, *J. Electrochem. Soc.* **2021**, *168*, 120514.
[41] Y.-K. Sun, S.-T. Myung, B.-C. Park, J. Prakas, I. Belharouak, K. Amine, *Nat. Mater.* **2009**, *8*, 320.
[42] Y.-K. Sun, Z. Chen, H.-J. Noh, D.-J. Lee, H.-G. J. Y. Ren, S. Wang, *Adv. Funct. Mater.* **2010**, *20*, 485.
[43] Y.-K. Sun, Z. Chen, H.-J. Noh, D.-J. Lee, H.-G. J. Y. Ren, S. Wang, C.-S. Yoon, S.-T. Myung, K. Amine, *Nat. Mater.* **2012**, *11*, 942.
[44] C. Yoon, K.-J. Park, U.-H. Kim, H.-H. Ryu, Y.-K. Sun, *Chem. Mater.* **2017**, *29*, 10436.
[45] N. Zhang, N. Zaker, H. Li, A. Liu, J. Inglis, L. Jing, J. Li, Y. Li, G. Botton, J. Dahn, *Chem. Mater.* **2019**, *31*, 10150.
[46] Y. Liu, H. Wu, Y. Wang, K. Li, S. Yin, J. Dahn, *J. Electrochem. Soc.* **2021**, *167*, 160556.
[47] W. Li, H.-Y. Asl, Q. Xie, A. Manthiram, *J. Am. Chem. Soc.* **2019**, *141*, 5097.
[48] A. Grenier, P. Reeves, H. Liu, I. Seymour, K. Märker, K. WiadereK, P. Chupas, C. Grey, K. Chapman, *J. Am. Chem. Soc.* **2020**, *142*, 7001.
[49] L. Zou, Z. Liu, W. Zhao, H. Jia, J. Zheng, Y. Yang, G. Wang, J. Zhang, C. Wang, *Chem. Mater.* **2018**, *30*, 7016.
[50] H. Sun, A. Manthiram, *Chem. Mater.* **2017**, *29*, 8486.
[51] J. Liao, A. Manthiram, *J. Power Sources* **2015**, *282*, 429.
[52] H. Zhang, B. May, F. Omenya, S. Whittingham, J. Cabana, G. Zhou, *Chem. Mater.* **2019**, *31*, 7790.
[53] S. Hwang, W. Chang, S. Kim, D. Su, D.- H. N. Kim, J.-Y. Lee, K.-Y. Chung, E. A. Stach, *Chem. Mater.* **2014**, *26*, 1084.
[54] C. Geng, D. Rathore, D. Heino, N. Zhang, I. Hamam, N. Zaker, G. Botton, R. Omessi, N. Phattharasupakun, T. Bond, C. Yang, J. Dahn, *Adv. Energy Mater.* **2022**, *12*, 2103067.
[55] C. Xu, K. Märker, J. Lee, A. Mahadevegowda, P. Reeves, S. Day, M. Groh, S. Emge, C. Ducati, B. Mehdi, C. Tang, C. Grey, *Nat. Mater.* **2021**, *20*, 84.
[56] M. Bianchini, M. Roca-Ayats, P. Hartmann, T. Brezesinski, J. Janek, *Angew. Chem., Int. Ed.* **2018**, *58*, 10434.
[57] L. de Biasi, A. Schiele, M. Roca-Ayats, G. Garcia, T. Brezesinski, P. Hartmann, J. Janek, *ChemSusChem* **2019**, *12*, 2240.
[58] S. Ahmed, M. Bianchini, A. Pokle, M.-S. Munde, P. Hartmann, T. Brezesinski, A. Beyer, J. Janek, K. Volz, *Adv. Energy Mater.* **2020**, *10*, 2001026.
[59] M. Mock, M. Bianchini, F. Fauth, K. Albe, S. Sicolo, *J. Mater. Chem. A* **2021**, *9*, 14928.
[60] C. Delmas, M. Ménétrier, L. Croguennec, S. Levasseur, J. P. Péres, C. Pouillerie, G. Prado, L. Fournès, F. Weill, *J. Inorg. Mater.* **1999**, *1*, 11.
[61] L. Croguennec, C. Pouillerie, A. Mansour, C. Delmas, *J. Mater. Chem.* **2001**, *11*, 131.
[62] N. Ikeda, I. Konuma, H.-B. Rajendra, T. Aida, N. Yabuuchi, *J. Mater. Chem. A* **2021**, *9*, 15963.
[63] L. Croguennec, C. Pouillerie, C. Delmas, *J. Electrochem. Soc.* **2000**, *147*, 1314.
[64] F. Fauth, I. Peral, C. Popescu, M. Knapp, *Powder Diffr.* **2013**, *28*, S360.